JMEPEG (2010) 19:1161–1171
DOI: 10.1007/s11665-009-9589-1

1059-9495/$19.00

Tensile and Fatigue Behavior of Friction-Stir Welded Tailor-Welded Blank of Aluminum Alloy 5754

M. Garware, G.T. Kridli, and P.K. Mallick

(Submitted November 4, 2008; in revised form October 16, 2009)

Friction stir welding is becoming increasingly desirable in many applications, including tailor-welded blanks in which two sheets of different thicknesses are joined together to form blanks that can be subsequently stamped into a final product shape. In this article, we have studied the static tensile and tension-tension fatigue behavior of friction stir welded joint in a tailor-welded blank of aluminum alloy 5754. It was observed that the yield and tensile strengths of friction stir welded specimens with weld located 90° to the tensile direction are close to the base material values, but its elongation is nearly half the elongation for the base material. The friction stir welded joints had relatively high-fatigue strength, and was even superior to that of the base aluminum alloy in the high-cycle region. Pre-straining caused by press forming lowered the elongation to failure, but improved the fatigue performance.

Keywords fatigue, friction stir welding, pre-straining, tailor-welded blanks

1. Introduction

Tailor-welded blank or TWB is obtained by welding two sheets of different thicknesses or different materials to form a single sheet that can be subsequently stamped to make the final shape. The use of tailor-welded blanks allows thickness variation or material variation in the same blank, which can be utilized to vary stiffness or strength in local areas of a structure. Tailor-welded blanks are of great interest to the automotive industry, since they can be used in weight savings of many stamped body panels and body structures, such as floor pan, door inner panel, roof reinforcement, and front rail structure (Ref 1).

The welding process used for making aluminum tailor-welded blanks includes laser welding, mash seam welding, and gas tungsten arc welding. In recent years, friction stir welding has been gaining significant attention in the automotive industry (Ref 2, 3) and has also been considered for making tailor-welded blanks of aluminum (Ref 4). In friction stir welding, a rotating tool, consisting of a smaller diameter pin-shaped probe and a larger diameter shoulder, is traversed under pressure along the interface between the two sheets being joined. The frictional heat generated by the rotating tool produces a thermally softened region at the interface and the adjoining area. The softened material is forced to flow in a rotary motion on the surface as well as in the interior by the rotating tool. As the material flowing around the tool coalesces, a butt weld is formed. The weld is formed without melting the material, as such any problems associated with melt solidification from fusion welded joints are greatly minimized and/or eliminated.

The early research on aluminum tailor-welded blanks for automotive applications concentrated on the weld line behavior, such as weld cracking and weld-line shift, during stamping (Ref 5-7). Since tailor-welded blanks are increasingly used in structural components, their mechanical properties must also be characterized. While some research on the static tensile behavior of aluminum TWB has been published (Ref 5, 8), there is limited published data on their fatigue behavior. Davies et al. (Ref 6) reported the fatigue behavior of tailor-welded blanks of 1 and 2 mm thick AA5182-O sheets. In their study, the butt welds were formed using gas tungsten arc welding and non-vacuum electron beam welding methods. In both cases, the welded area contained varying amounts of porosity, undercuts, and lack of fusion. They observed that if the weld was produced with low levels of these defects, the fatigue S-N diagram of the welded joint transverse to the loading direction was nearly identical to that of the monolithic sheet.

Fatigue of friction stir welded joints in plates of similar thickness has been reported in recent literature (Ref 9-13). Ericsson and Sandström (Ref 9) and Zhou et al. (Ref 10) have shown that the fatigue performance of friction stir welded joints in aluminum alloys, such as AA 5083, are far superior than that of metal inert gas (MIG) or tungsten inert gas (TIG) welded joints. In most of these studies, the plate thickness was 4 mm or greater, and the emphasis has been on the effect of welding parameters, especially the welding speed, on the fatigue life of friction stir welded joints. It was observed that welding speed did not affect fatigue life significantly.

The objective of this article is to report the tensile and fatigue behavior of tailor-welded blanks of aluminum alloy AA5754. Friction stir welding was used to manufacture the tailor-welded blanks in this research. Since tailor-welded blanks undergo stretching during stamping operation, it was also decided to examine the tensile and fatigue performance of the friction stir welded joints after tensile pre-strains. The effect of weld-line orientation relative to the loading direction has also been considered.

M. Garware, G.T. Kridli, and **P.K. Mallick**, Center for Lightweighting Automotive Materials and Processing, University of Michigan-Dearborn, Dearborn, MI 48128. Contact e-mail: pkm@umich.edu.

2. Experimental

The TWB considered in this investigation was made by friction stir welding 1.06 and 1.66 mm thick AA5754 sheets. This alloy is not a heat-treatable aluminum-magnesium alloy with nominal Mg content in the range of 2.6-3.6%. Table 1 shows the nominal composition of AA5754 as registered with The Aluminum Association (Ref 14). The TWB consisted of a 1.66 mm thick AA5754 sheet in the center of the blank that was friction stir welded to 1.06 mm thick AA5754 sheets on the sides as shown in Fig. 1(a). Both friction stir weld lines were normal to the rolling direction and they ran in opposite directions (Fig. 1b). A schematic of the weld cross section is shown in Fig. 1(c). The welding process left a keyhole at the end of each weld line, which was formed when the welding tool exited the sheets. Micrographs of the weld, shown in Fig. 2, indicate that, as a result of the heating and stirring process, dynamic recrystallization occurred in the weld zone, leading to a finer grain size in the

Table 1 Alloying elements and their nominal weight percentage in AA5754 (Ref 14)

Mg	Mn	Fe	Si	Cr	Zn	Ti	Cu
2.6-3.6	0.50	0.40	0.40	0.30	0.20	0.15	0.10

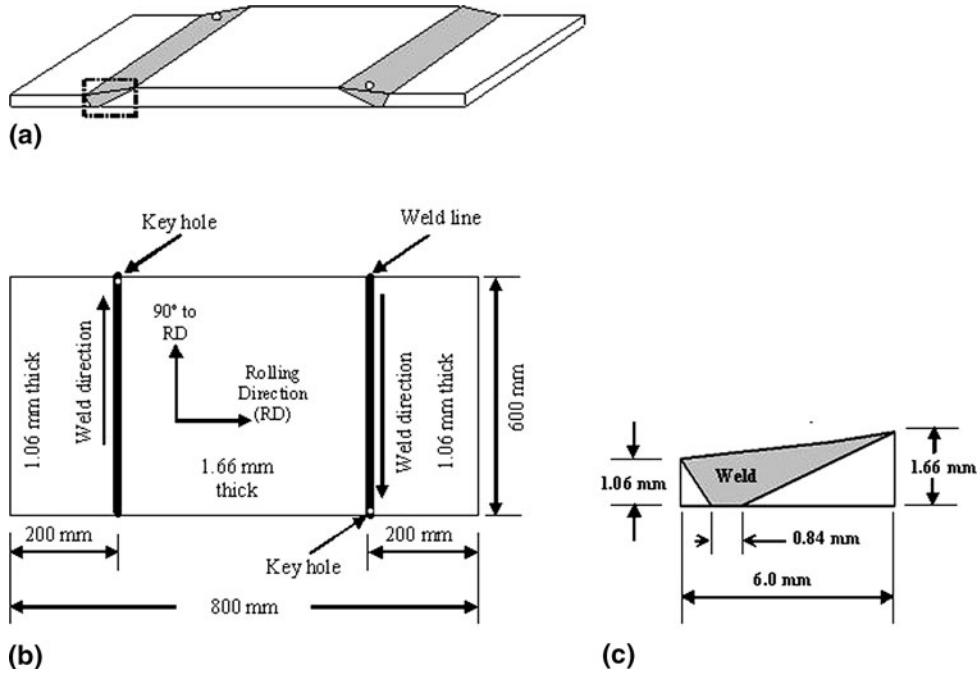

Fig. 1 (a) Schematic of the tailor-welded blank, (b) top view of the TWB, and (c) weld cross section through the thickness of the TWB showing the general weld dimensions

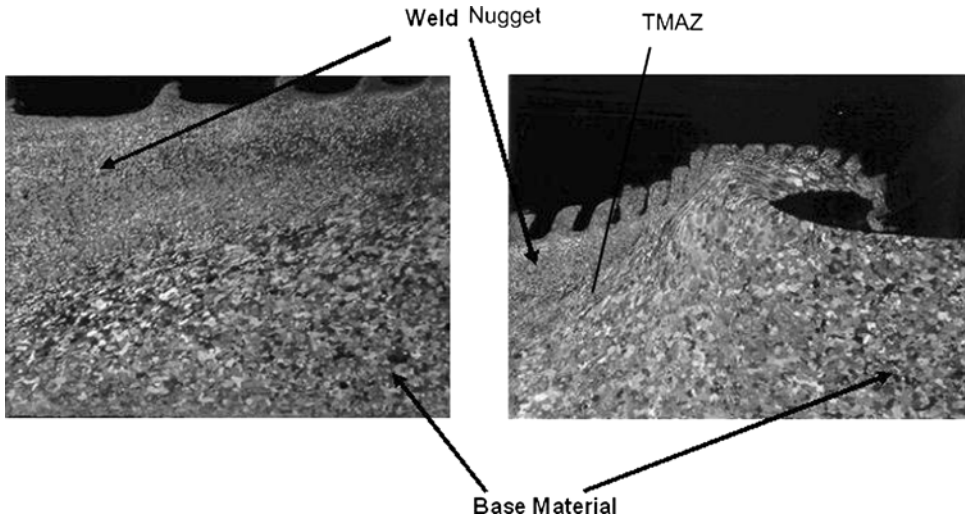

Fig. 2 Micrographs of the weld and the base material

weld material compared with that of the base material. Between the base material and the weld center, there is evidence of thermo-mechanically affected zone (TMAZ) where the grains appear to be elongated. The tool marks left on the surface of TWB are also visible in Fig. 2. This agrees with observations reported in the literature (Ref 11, 13, 15-17).

2.1 Tension Tests

Figure 3(a) shows the ASTM E-8 sub-size specimen used for tensile tests. Conventional machining process, such as milling, was not used to make the specimens to avoid the possibility of introducing machining-induced stresses and chatter-induced microcracks in the welded area. The specimens were prepared by water-jet cutting, which was less expensive compared to the other non-conventional machining processes, such as laser cutting. Additionally, water jet cutting does not result in thermal changes to the machined edge of the specimen. However, the edges of the water jet cut specimens were rough. They were deburred and cleaned using a machinist's stone and emery cloth (Scotchbrite©).

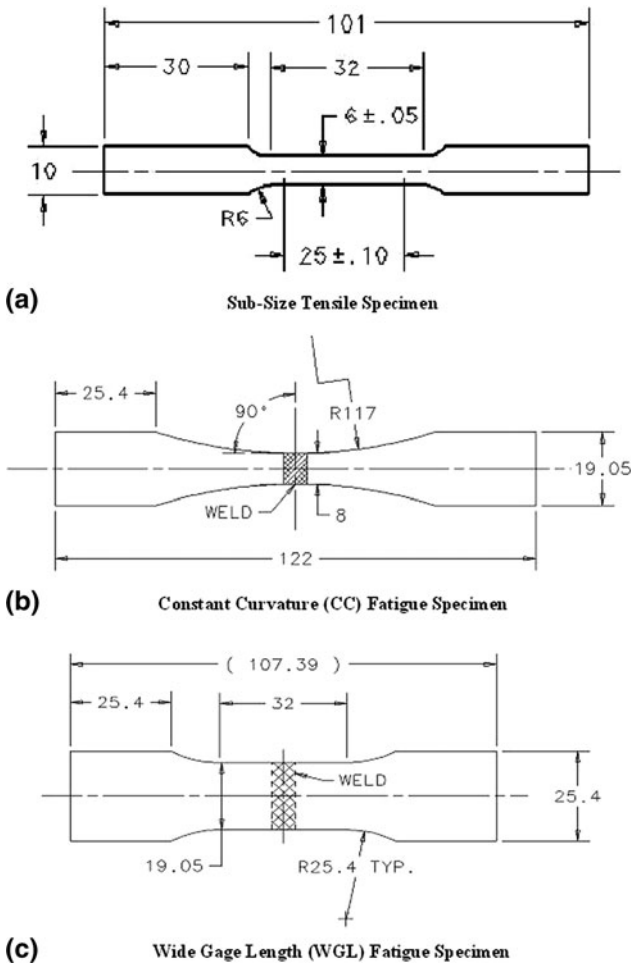

Fig. 3 Schematics of the tensile and fatigue specimens (all dimensions are in mm)

Tensile tests were performed on an Instron tensile testing machine at a crosshead speed of 5 mm/s. The un-welded specimens were obtained from the thinner side of the TWB, measuring 1.06 mm in thickness. The un-welded specimens were prepared such that the rolling direction was at 0°, 45°, and 90° to the tensile loading direction. The tensile specimens with the welded joint, henceforth referred to as the TWB specimens, were prepared such that the weld orientation was at 0°, 45°, and 90° to the tensile loading direction (Fig. 4). For the TWB specimen with the weld-line at 90°, the rolling direction was at 0° to the loading direction. For the weld-line at 0°, the rolling direction was at 90° to the loading direction. Finally, for the weld-line at 45°, the rolling direction was at 45° to the loading axis. This is schematically shown in Fig. 4.

To prepare the specimens with tensile pre-strain, the TWB specimens were cut into 178 by 178 mm square blanks using a shearing machine. These blanks were electrochemically etched with 2.5 by 2.5 mm square grids over the entire surface. Flat-bottomed cylindrical cups were stamp-formed from these blanks. The grid dimensions were measured using a tool-maker's microscope. From these measurements, it was observed that the strain induced in the cup was between 2.5 and 9.25%. A photograph showing the formed cup is shown in Fig. 5. The ASTM E-8 sub-size specimens were prepared from the center of these cups using water-jet cutting. The weld line in the specimen was positioned at 90° to the axial direction of the specimen (which was also the rolling direction) and was located at the mid-length of the specimen.

Finite element analysis (FEA) of the uniaxial tests was carried out using ABAQUS finite element software with the objective of determining the effect of the presence of weld on the stress and strain distributions in the TWB tensile specimen. The dimensions of the modeled specimen are as shown in Fig. 3(a), with a weld in the center of the gage of the specimen and perpendicular to the loading direction. The weld profile modeled for the FEA is shown in Fig. 1(c). Solid 3-D elements of the 1st order with 8 nodes were used in the model. In the gage section, which included the weld region, the element size

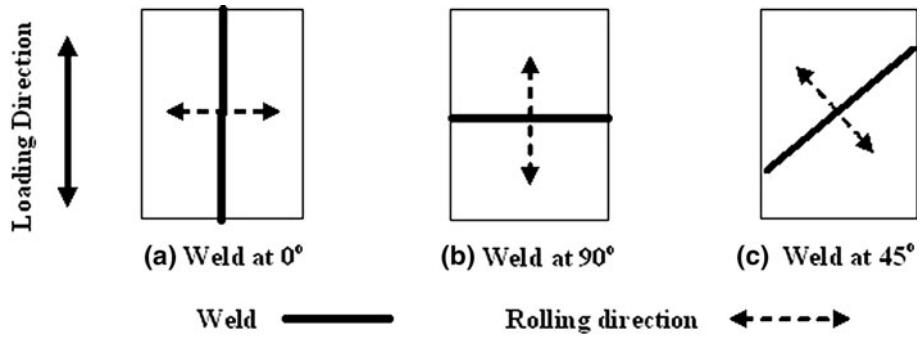

Fig. 4 Schematic showing weld and rolling directions in the TWB specimens relative to the loading direction

was 1.118 by 2.54 by 0.315 mm. The base material properties and the weld material properties were assumed to be the same as given by Kridli et al. (Ref 5) for an AA5182 alloy. They were: elastic modulus = 71 and 68 GPa, yield strength = 132 and 146 MPa, ultimate tensile strength (UTS) = 280 and 256 MPa, strength coefficient (K) = 551.5 and 453.5 MPa, power law exponent (n) = 0.33 and 0.23 for the base material and the weld material, respectively. Since the weld material properties were available for the 5182 alloy, it was used in the FEA instead of the 5754 alloy. The effect of bending due to the gage mismatch in the TWB was considered in the model. In an actual tension test, closing the grips on the specimen ends at the beginning of the test induced bending due to the misalignment of the thin and the thick sheets making up the TWB (Fig. 1a). To account for bending, the analysis was run in two steps. In the first step, nodes in the grip section of the thin side of the TWB were displaced such that the mid-plane of the thin side grip coincided with the mid-plane of the thick side in order to simulate actual grip closing experienced by the specimen. In the second step, displacement was applied to stretch the specimen along the loading axis.

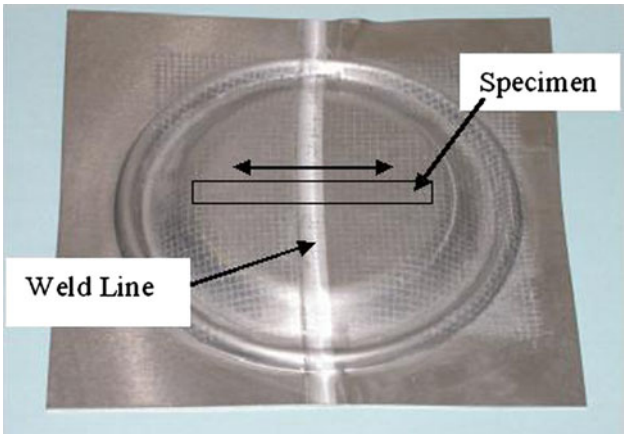

Fig. 5 Specimen orientation in the formed flat-bottomed cup

Table 2 Average tensile properties of AA5754

Property	Longitudinal specimen	45° Specimen	Transverse specimen
Yield strength, MPa	94.74 ± 2.38	96.72 ± 8.75	100.17 ± 12.73
UTS, MPa	232.83	226.80	230.63
K value, MPa	482.27	450.67	455.33
n value	0.31	0.30	0.29
Uniform elongation, %	18.33	22.34	21.83
Elongation to fracture, %	21.22	25.81	25.44

2.2 Fatigue Tests

Two types of specimens were used for fatigue tests as shown in Fig. 3(b) and (c). The constant curvature (CC) specimens were used to study the effect of weld location along the length of the specimen. The wide gage length (WGL) specimens were used to study the effect of weld orientation at 45° and 90° to the loading direction. In the CC specimens, the weld was located either at the mid-length or 18 mm off-centered from the mid-length. In the off-centered specimens, the narrowest cross section was at the mid-length and the weld was located either on the thick side or on the thin side of the specimen.

Fatigue tests were carried out using an MTS 810 servo-hydraulic testing machine. Tension-tension mode of load application was used using a sine wave of frequency 20 Hz. The ratio of the minimum stress to the maximum stress (R) was 0.1. The maximum stress levels used were 50, 60, 70, and 80% of the UTS of the respective specimen type, given in Table 2 and 3. The load corresponding to the maximum stress level was calculated based on the smallest cross-sectional area of each specimen. The thinner end of the TWB specimens was taped with six layers of 0.1 mm thick tape to account for the thickness difference and to reduce the effect of bending. The specimens were subjected to fatigue cycling either to failure or to a maximum of 2,000,000 cycles, whichever occurred first. Three specimens were tested at each stress level.

3. Results

3.1 Tension Test Results

The tensile properties of the AA5754 alloy are presented in Table 2. The tensile specimens were obtained from areas away from the welded area. The longitudinal specimens were parallel to the rolling direction and the transverse specimens were normal to the rolling direction. Each property value in this table represents the average of three specimens. Typical engineering stress-strain curves of these specimens are shown in Fig. 6. As can be seen from both Table 2 and Fig. 6, the difference in tensile properties in the three different directions considered is relatively small.

The TWB specimens were tested with weld orientations at 0°, 45° and 90° to the loading direction. Three specimens of each type were tested. Figure 7 shows samples of fractured test specimens for the three different weld orientations, with arrows indicating the weld location. It should be noted that the weld runs along the entire gage section in Fig. 7(c). The failure

Table 3 Average tensile properties of friction stir welded TWB of AA5754

Property	Original			Pre-strained (formed), weld at 90°
	Weld at 90°	Weld at 45°	Weld at 0°	
Yield strength, MPa	111.10 ± 7.48	109.50 ± 3.87	129.56 ± 6.69	192.2
UTS, MPa	226.10	215.48	225.72	228.5
Uniform elongation, %	9.03	8.72	19.35	3.37
Elongation to fracture, %	11.60	12.31	24.04	7.03

location of the 45° and 90° specimens was always on the thin gage side of the base material between the weld and the curved shoulder of the specimen as shown in Fig. 7.

Finite element analysis of the 90° TWB tensile specimen showed that much of the deformation takes place on the thin side. As can be seen in Fig. 8, the highest strain location is on the thin side of the specimen outside of the weld line. Furthermore, Fig. 8 shows that the thick side of the TWB specimens experience little or no deformation compared with the thin side. If it is assumed that the effective gage length of the TWB specimen is equal to the length of its thin side, i.e., half the total gage length, its uniform elongation will be half the uniform elongation value of the unwelded longitudinal specimen. This value is 9.16%, which is close to the observed value of 9.03% for the 90° TWB tensile specimen (Table 3).

The load-displacement curves of the TWB specimens are shown in Fig. 9. The average property values of the TWB specimens are presented in Table 3. The cross-sectional area of the thin side was used to calculate the stress in the 45° and 90° specimens. For the 0° specimens, the weld profile was taken into account to calculate the tensile stress. Comparing Table 2 and 3, it can be observed that the yield strengths of the 45° and 90° TWB specimens were higher than the yield strength of the un-welded specimens, but their uniform elongation and the elongation at fracture were approximately one-half of the corresponding elongation of the un-welded specimens. In these specimens, failure occurred on the thin gage side and much of the deformation took place on the thin gage side. The 0° TWB specimens with the weld line running longitudinally along the centerline showed tensile properties very similar to those of the un-welded specimens. The lower elongation at fracture values for the 45° and the 90° TWB specimens can be attributed to the fact that the majority of deformation in these specimens occurred on the thin side. Thus, elongation to fracture should be calculated based on the length of the thin side of the specimen, which is half the length of the gage section of each specimen. This would lead to elongation at fracture values comparable to the specimens with weld at 0°.

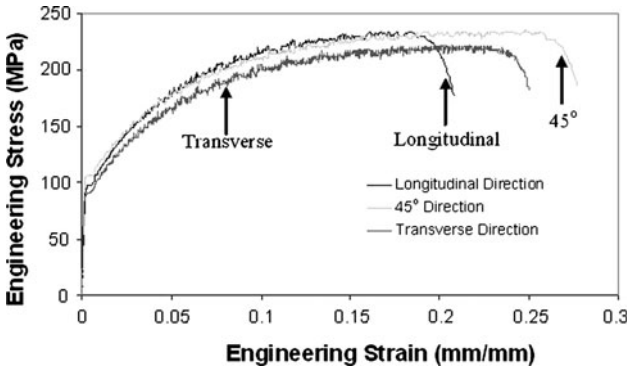

Fig. 6 Engineering stress-strain curves of AA5754

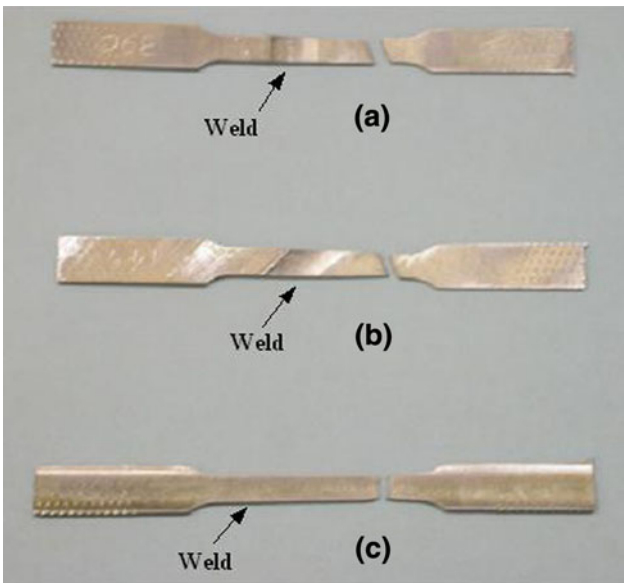

Fig. 7 Photographs showing failure location in TWB tensile specimens. (a) Weld at 90°; (b) weld at 45°; and (c) weld at 0° to loading direction

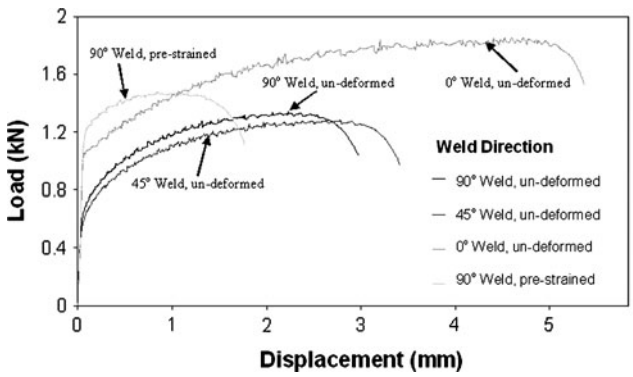

Fig. 9 Load-displacement curves of TWB specimens

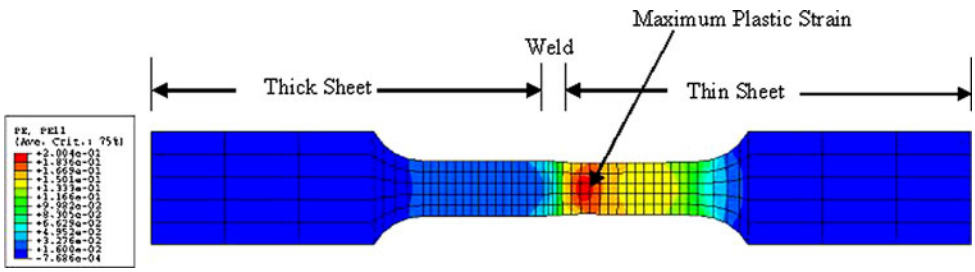

Fig. 8 Maximum predicted plastic strain in uniaxial tension of a TWB tensile specimen with the weld at the center of the gage section and perpendicular to the loading axis of the specimen

Figure 9 also shows the load-displacement curve of a pre-strained TWB specimen in which the weld was at 90° to the loading direction. Out of the three pre-strained specimens, one failed at a very small displacement compared to the other two. This specimen also failed in the weld, while the other two specimens failed on the thin side of the specimen. The average tensile properties of the two specimens that showed similar load-displacement curves are listed in Table 3. The average yield strength of the pre-strained TWB specimens was significantly higher; however, the average uniform elongation and elongation at fracture were significantly lower compared to the 90° TWB specimens.

3.2 Tensile Property of the Weld Material

Abdullah et al. (Ref 18) used the rule of mixtures equation to determine the weld material properties from the tensile test data of 0° TWB specimens with the weld line running along the tensile specimen axis. Following their approach, the rule of mixtures equation was also used here to estimate the yield strength of the friction stir weld.

$$S_w = \frac{S_0 A_0 - S_b A_b}{A_w} \quad \text{(Eq 1)}$$

In Eq (1), S_w, S_0, and S_b represent the strengths of the weld material, 0° TWB specimen and base material, respectively. The corresponding cross-sectional areas in the 0° TWB specimens are given by A_w, A_0, and A_b, respectively. Two types of 0° TWB specimens were used in this work to determine the weld material properties: (1) 6 mm wide sub-size specimens (Fig. 3a) and (2) 19 mm wide gage specimens (with dimensions similar to the specimen shown in Fig. 3c). The major difference between these types of specimens was the ratio of the weld area to the specimen area, which was 0.60 for the sub-size specimens and 0.20 for the wide gage specimens. Table 4 gives the tensile properties of these two types of specimens and the weld material properties derived using Eq (1). As can be seen in this table, there were slight differences in the tensile properties of the two types of specimens considered. Even though the weld material content in the sub-size specimen was higher, it produced lower values of both yield strength and UTS. Nevertheless, the yield strength of the weld material was significantly higher than that of the base material in both cases and the UTS of the weld material was in the same range as that of the base material.

3.3 Fatigue Test Results

Figure 10 shows the S-N curves of the un-welded AA5754 specimens prepared from areas away from the welded area on the thin side of the TWB. Figure 10 shows the results for the two types of fatigue test specimens described in section 2.2. Twelve specimens of each type were tested at four different

Table 4 Calculated weld material properties

			Weld material properties	
Property	**Sub-size specimen**	**Wide gage specimen**	**From sub-size specimen**	**From wide gage specimen**
Yield strength, MPa	129.56	115.33	149.27	175.84
UTS, MPa	225.72	237.67	222.43	265.78
Uniform elongation, %	19.35	21.50	…	…
Elongation at fracture, %	24.04	24.03	…	…

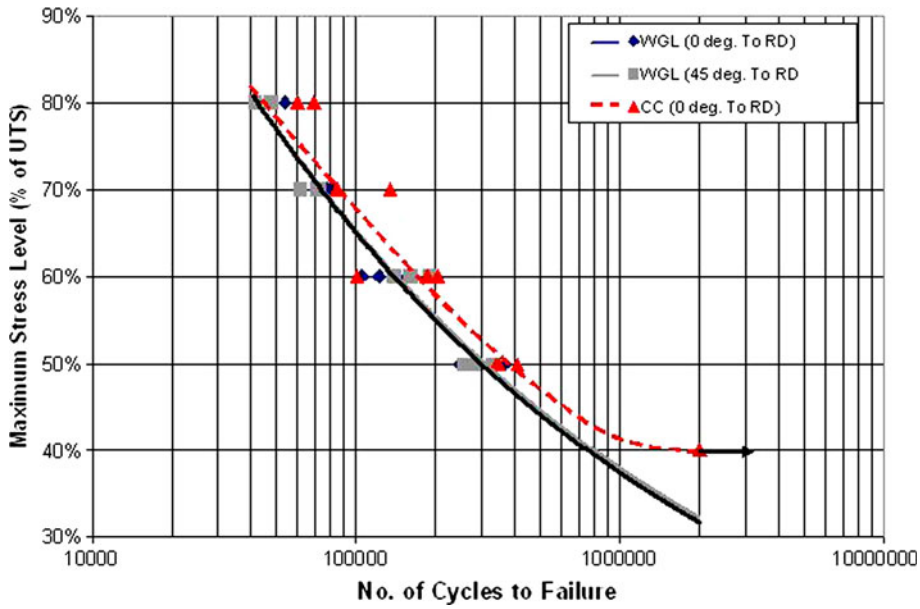

Fig. 10 S-N curves of AA5754

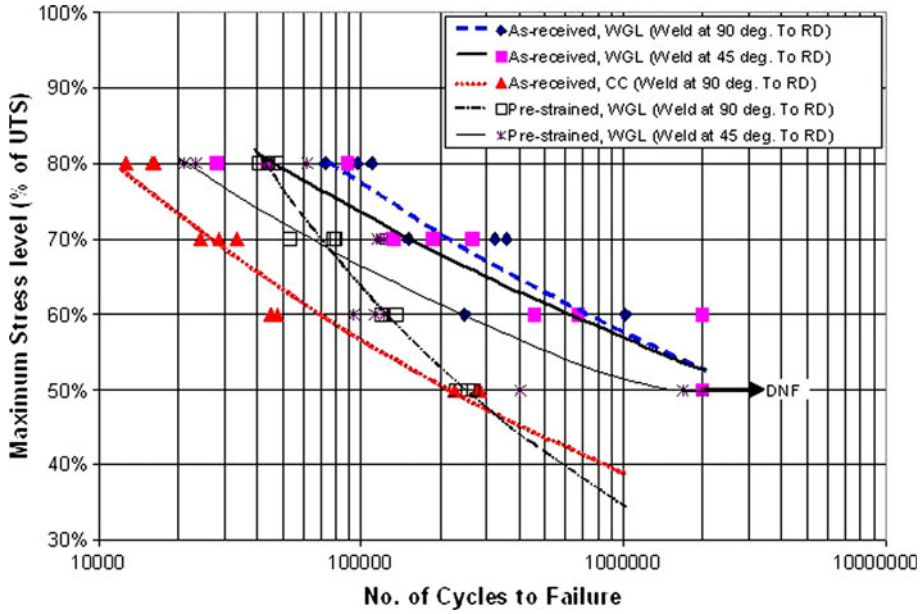

Fig. 11 S-N curves of TWB specimens

maximum cyclic stress levels, namely 80, 70, 60, and 50% of the UTS values given in Table 2. In addition, one specimen was tested at 40% of UTS, which did not fail in 2×10^6 cycles. All WGL specimens failed at or near the end of the gage length, while the CC specimens failed at the mid-length, which was also the smallest cross-sectional area. As can be seen in Fig. 10, there was very little difference between the S-N curves of 0° and 45° WGL specimens. However, the 0° CC specimens showed longer fatigue life at all cyclic stress levels.

Figure 11 shows the S-N curves of the two types of TWB specimens considered: (1) WGL specimens with welds oriented at 45° and 90° to the loading direction and (2) CC specimens with weld oriented at 90° to the loading direction. Twelve specimens of each type were tested at the same four different maximum stress levels shown in Fig. 10. The UTS values of these specimens are given in Table 3. Both WGL and CC specimens with the 90° weld at the center failed at the weld (Fig. 12a, b). The WGL specimens with weld at a 45° angle failed on the thin side near the end of the gage length.

In another set of fatigue tests, CC specimens containing weld at 90° to the loading direction, but shifted to either the thick side or the thin side of the specimen were considered. The specimens with the weld shifted toward the thick side failed on the thin side of the base material, where the cross-sectional area was the smallest (Fig. 12c). In the specimens with the weld shifted toward the thin side, the smallest cross-sectional area was not at the mid-length, but at the weld region. All specimens of this kind failed at the weld region (Fig. 12d). The S-N curves of these specimens are compared with that of the CC specimens with weld at the mid-length in Fig. 13.

The final fatigue tests were conducted with the pre-strained TWB specimens. These were WGL specimens with weld at either 45° or 90° to the loading direction. The specimens with 45° weld failed on the thin side of the base material, away from the weld; however, the specimens with 90° weld all failed at the weld. As can be seen in Fig. 11, the S-N behavior of the pre-strained specimens was significantly superior to that of the TWB specimens without any pre-strains.

During microscopic analysis to determine the cross-sectional area of the weld, it was observed that the weld profile at the end of the weld line was not the same as that at the start. For example, at the end of the weld (approximately 50 mm from the keyhole), there was a small depression or valley at the intersection of the weld material and the thinner side of blank (Fig. 14). This valley was not observed at the start of the weld and could have been a result of heat building up ahead of the tool, which softened the thin material and led to the friction stirring tool "plowing" into the thin side of the TWB. The presence of the valley indicated that another factor affecting the fatigue behavior of the TWB might be the location of the weld along the tool path. In order to study this effect, six specimens of the CC type with weld at 90° taken from the start of the weld and six specimens taken from the end of the weld were fatigue tested at 60 and 80% stress levels. All of these specimens failed at the weld region. At 60% stress level, the average fatigue life of the start-of-the-weld specimens was 140,220 cycles (2 specimens) and that of the-end-of-the-weld specimens was 144,970 cycles (3 specimens). On the other hand, at 80% stress level, the average fatigue life of the start-of-the-weld specimens was 68,030 cycles (3 specimens) compared to only 10,320 cycles (3 specimens) for the end-of-the-weld specimens. Thus, the fatigue data indicate that the end-of-the-weld specimens had considerably lower fatigue life at the higher stress level, but at the lower stress level, there was very little difference.

From the fatigue test results it can be noted that the introduction of the weld changes the fatigue behavior of the system. Two comparisons are made here. The first is between the un-welded AA5754 specimens and the TWB specimens. In the TWB specimens, the weld was at 90° to the loading direction. The comparison is shown in Fig. 15, which shows that at maximum stress levels greater than 65% of the static strength, the TWB specimens had lower fatigue life than the un-welded specimens. At maximum stress levels lower than 65% of the static strength, the TWB specimens had higher fatigue life than the un-welded specimens. Thus, it appears that

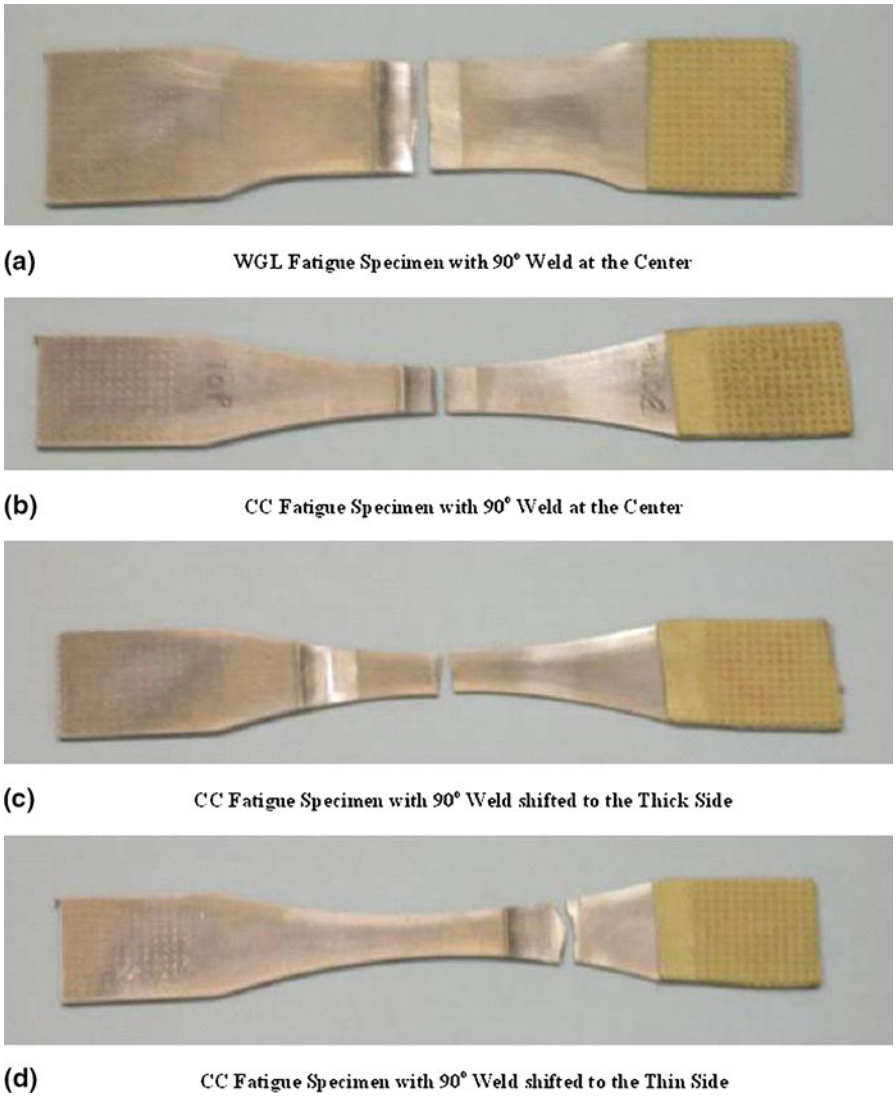

Fig. 12 Photographs showing failure location in TWB fatigue specimens with 90° weld

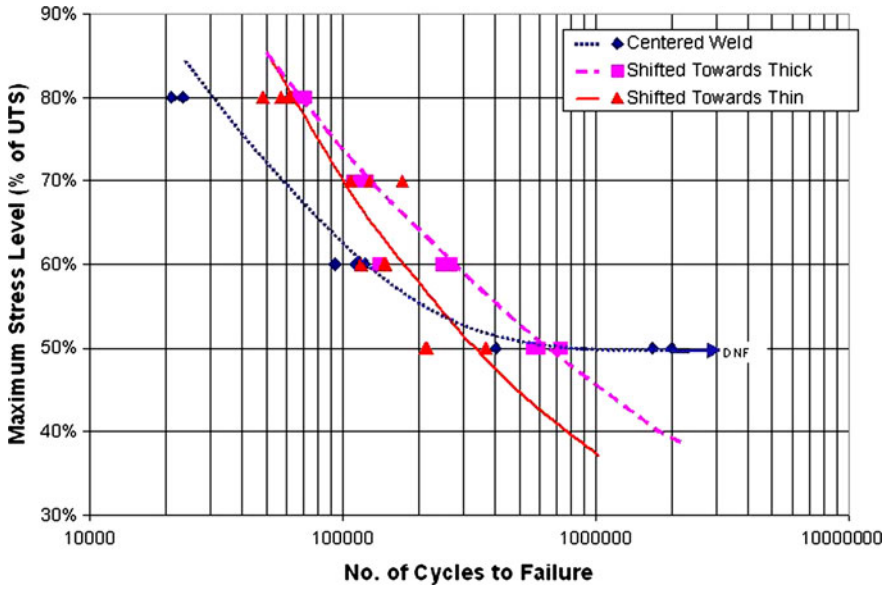

Fig. 13 S-N curves for TWB fatigue specimens with shifted weld locations

the welded joint was weaker in fatigue than the base material at high stress levels, but stronger in fatigue than the base material at low stress levels.

The second comparison considers the effect of forming pre-strain on the fatigue life of TWB specimens. Both undeformed and formed (pre-strained) specimens were of the WGL type and had the weld at 90° to the loading direction. As shown in Fig. 16, the formed (pre-strained) TWB specimens performed better under fatigue loading than the undeformed TWB specimens at both higher and lower stress levels. This observation agrees with the general effect of work hardening, which leads to an increase in fatigue life. Thus, pre-straining caused by forming seems to have a beneficial effect.

The difference in the tensile and fatigue properties of unwelded and TWB specimens in our study can be explained in terms of the possible compressive residual stress pattern in the weld area. There are two thermo-physical phenomena that contribute to the strength of friction stir welded joints: (1) friction generated heat at the tool-work piece interface that causes recrystallization and a reduction in hardness in the weld nugget and the surrounding area, and (2) thermal constraints between the weld area and the base material during the cooling phase that give rise to residual stresses in the weld area (Ref 15). If the friction stir welded joint is between two plates of equal thicknesses, both longitudinal and transverse residual stresses are found to be tensile in the weld area and compressive outside the weld area (Ref 15, 19). Similar residual stress pattern was also observed by Clapham et al. (Ref 20) in laser welded TWB specimens when the sheets on both sides of the joint were of the same thickness, which in their case was 1.5 mm. However, when the laser welded joint was made between sheets of unequal thicknesses, which in their study were 1.5 mm on one side and 0.9 mm on the other side, the transverse residual stress became compressive in the weld area as well as outside the weld area. The reversal of transverse residual stresses in the weld area from tensile to compressive was attributed to the mechanical constraint provided by the thicker side relative to the thinner side. In our study, the TWB specimens had unequal thicknesses on two sides of the joint, and they showed higher yield strength and higher long-life fatigue strength. Following the observations made by Clapham et al. (Ref 20), it is possible that the compressive transverse residual stress in the weld area may have been the reason for achieving higher yield strength and higher long-life fatigue strength for our TWB specimens. Clapham et al. (Ref 20) also observed that when the welded TWB specimens with unequal sheet thicknesses were subjected to tensile pre-strains, the transverse residual stress remained compressive, albeit lower in value, with up to 3% pre-strain and became slightly tensile with 7% pre-strain. The improved fatigue performance of pre-strained TWB specimens in our study is possibly partly due to the compressive residual stresses created after welding, but

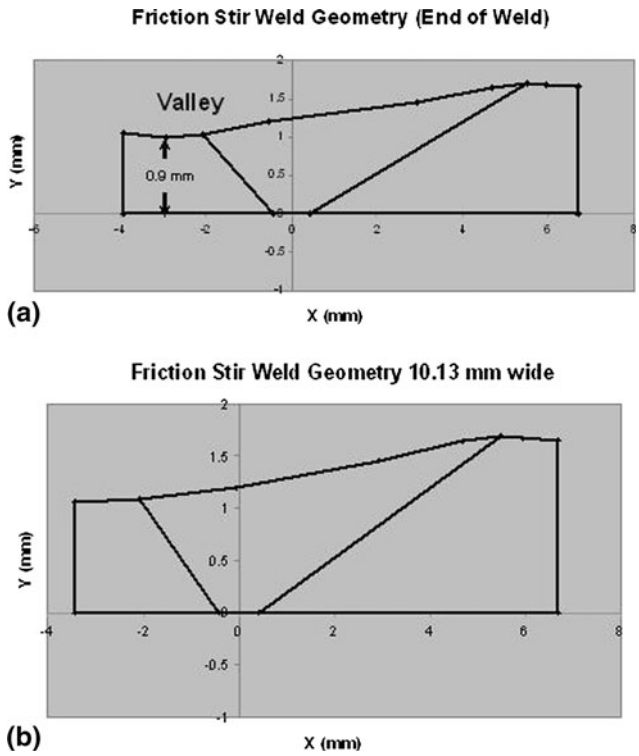

Fig. 14 (a) Weld geometry—end of weld (note the valley) and (b) start of the weld

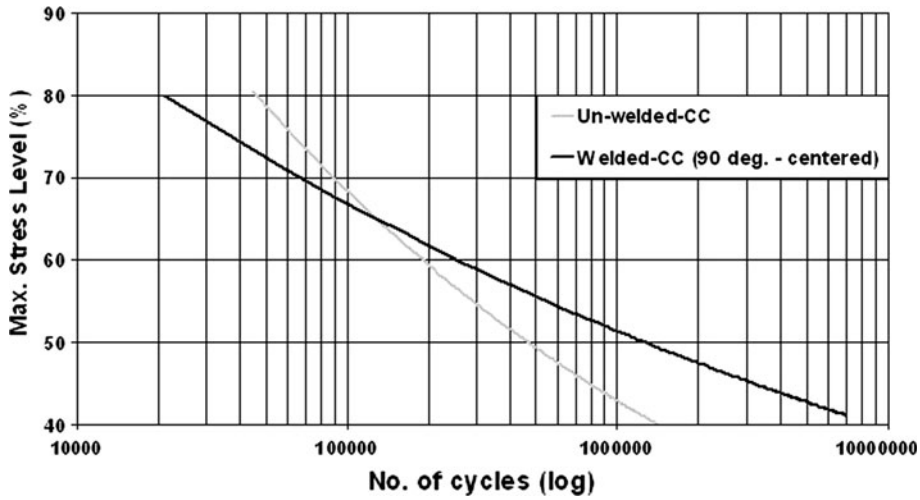

Fig. 15 Comparison of S-N curves of un-welded and welded AA5754 specimens (CC specimens). The weld was at the center and at 90° to the loading direction

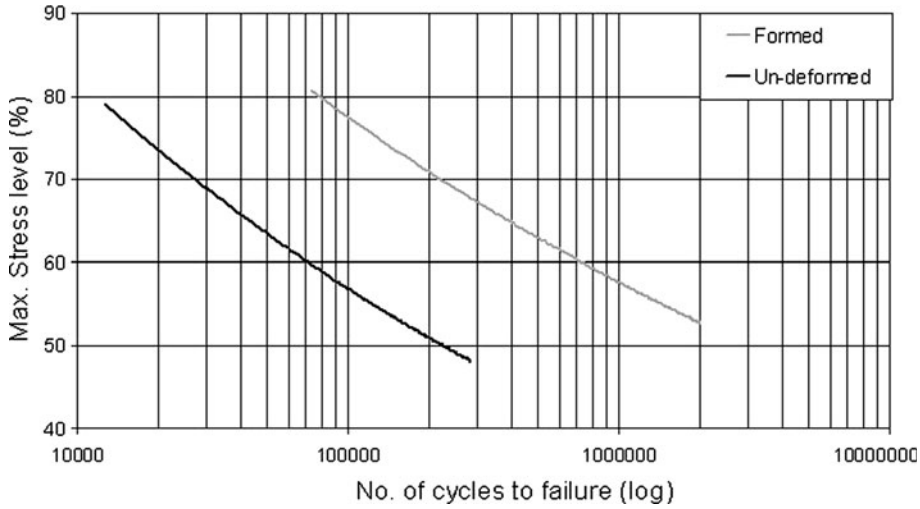

Fig. 16 Effect of forming (pre-straining) on the fatigue behavior of TWB specimens with weld at 90° (WGL specimens)

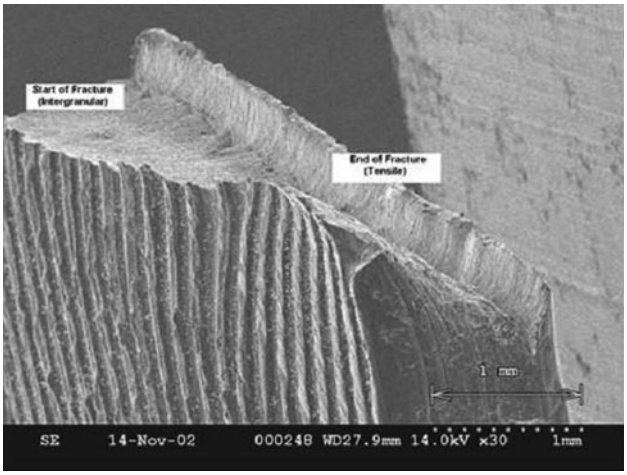

Fig. 17 Fracture surface of a TWB fatigue specimen with weld centered at 90° to the loading direction

may also be due to additional compressive residual stresses created due to differential deformations on the two sides of the weld line during the press forming operation.

3.4 Fatigue Fracture Surface Observations

Figure 17 shows the fracture surface of a CC fatigue specimen with a 90° weld at its mid length. The specimen was subjected to 50% stress level and failed at the weld at 1.683M cycles. Failure started in this specimen at the top right corner and progressed toward the left edge. The deep tool marks are clearly visible on the surface. There was also evidence of bending, which was caused due to load eccentricity resulting from thickness difference between the two sides of the specimen. The crack initiation was on the tension side of the specimen, from one of the tool marks. After the fatigue crack propagated nearly two-thirds of the specimen width with nearly flat, featureless surface, there was evidence of ductile crack propagation and shear lip formation. At higher magnifications, it was observed that initially the fatigue crack propagation was

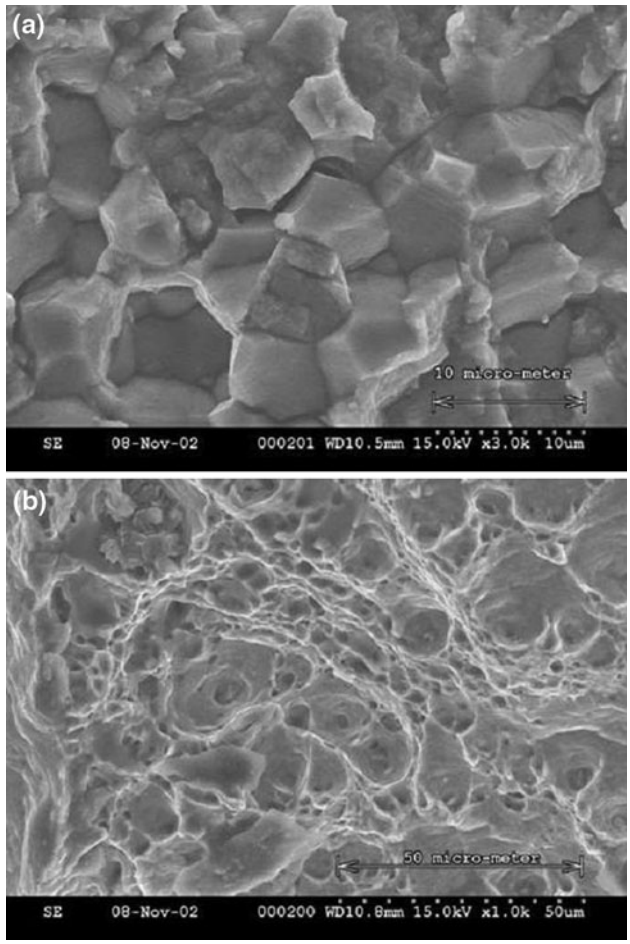

Fig. 18 SEM photographs of two regions on the fracture surface of a TWB fatigue specimen: (a) crack initiation area, (b) final crack propagation area

by intergranular crack growth (Fig. 18). In the ductile region, the fracture surface contained large number of dimples, which usually accompany ductile tensile failure in 5754 alloys.

4. Conclusions

In this article, we have studied the tension-tension fatigue behavior of friction stir welded joint in a tailor-welded blank of aluminum alloy 5754. Both tensile and fatigue failure in the tailor welded blank occurred on the thin gage side irrespective of the weld orientation with respect to the loading direction. It was observed that the friction stir welded joints had relatively high fatigue strength, and were even superior to that of the base aluminum alloy in the high cycle region. The fatigue failure appeared to have originated from the tool marks on the surface at the weld region. The valley created at the end of the weld line by tool ''plowing'' caused a reduction in fatigue performance. On the other hand, pre-straining caused by press forming tended to improve the fatigue performance.

Acknowledgments

The authors would like to thank Ford Motor Company for providing the material used in this investigation and the Henry Patton Center for Engineering Education and Practice at the University of Michigan-Dearborn for the financial support.

References

1. Auto/Steel Partnership, Tailor Welded Blank Design and Manufacturing Manual, Technical Report, 1995
2. T. Barnes and I. Ashby, Joining Techniques for Aluminum Spaceframes Used in Automobiles, Part I—Solid and Liquid Phase Welding, *J. Mater. Proc. Tech.*, 2000, **99**, p 62–71
3. W. Thomas and E. Nicholas, Friction Stir Welding for the Transportation Industries, *Mater. Des.*, 1997, **18**, p 269–273
4. S. Kallee and D. Nicholas, Application of Friction Stir Welding to Lightweight Vehicles, SAE Technical Paper Series, No. 982362, 1998
5. G.T. Kridli, P.A. Friedman, and A.M. Sherman, Formability of Aluminum Tailor-Welded Blanks, SAE Technical Paper Series, No. 2000-01-0772, 2000
6. R. Davies, G. Grant, M. Smith, and E. Oliver, Formability and Fatigue of Aluminum Tailor-Welded Blanks, SAE Technical Paper Series, No. 2000-01-2664, 2000
7. B. Kinsey, V. Viswanathan, and J. Cao, Forming of Aluminum Tailor Welded Blanks, *J. Mater. Manu.*, 2001, **110**, p 673–679
8. H.R. Shakeri, A. Buste, M.J. Worswick, J.A. Clarke, F. Feng, M. Jain, and M. Finn, Study of Damage Initiation and Fracture in Aluminum Tailor Welded Blanks Made Via Different Welding Techniques, *J. Light Metals*, 2002, **2**, p 95–110
9. M. Ericsson and R. Sandström, Influence of Welding Speed on the Fatigue of Friction Stir Welds, and Comparison with MIG and TIG, *Int. J. Fatigue*, 2003, **25**, p 1379–1387
10. C. Zhou, X. Yang, and G. Luan, Fatigue Properties of Friction Stir Welds in Al 5083 Alloy, *Scripta Mater.*, 2005, **53**, p 1187–1191
11. K.V. Jata, K.K. Sankaran, and J.J. Ruschau, Friction-Stir Welding Effects on Microstructure and Fatigue of Aluminum Alloy 7050-T7451, *Metall. Mater. Trans. A*, 2000, **31A**, p 2181–2192
12. T. Dickerson and J. Przydatek, Fatigue of Friction Stir Welds in Aluminum Alloys that Contain Root Flaws, *Int. J. Fatigue*, 2003, **25**, p 1399–1409
13. M.N. James, D. Hattingh, and G. Bradley, Weld Tool Travel Speed Effects on Fatigue Life of Friction Stir Welds in 5083 Aluminum, *Int. J. Fatigue*, 2003, **25**, p 1389–1398
14. The Aluminum Association, International Alloy Designations and Chemical Composition Limits for Wrought Aluminum and Wrought Aluminum Alloys, revised April 2006
15. M. Peel, A. Steuwer, M. Preuss, and P. Withers, Microstructure, Mechanical Properties and Residual Stresses as a Function of Welding Speed in Aluminum AA5083 Friction Stir Welds, *Acta Mater.*, 2003, **51**, p 4791–4801
16. M. Sutton, B. Yang, A. Reynolds, and R. Taylor, Microstructural Studies of Friction Stir Welds in 2043 T3 Aluminum, *Mater. Sci. Eng.*, 2002, **A323**, p 160–166
17. Y. Kwon, J. Shigematsu, and N. Saito, Mechanical Properties of Fine Grained Aluminum Alloy Produced by Friction Stir Process, *Scripta Mater.*, 2003, **49**, p 785–789
18. K. Abdullah, P.M. Wild, J.J. Jeswiet, and A. Ghasempoor, Tensile Testing for Weld Deformation Properties in Similar Gage Tailor Welded Blanks Using the Rule of Mixtures, *J. Mater. Proc. Tech.*, 2001, **112**, p 91–97
19. H. Lombard, D.G. Hattingh, A. Steuwer, and M.N. James, Effect of Process Parameters on the Residual Stresses in AA5083-H321 Friction Stir Welds, *Mater. Sci. Eng. A*, 2009, **501**, p 119–124
20. L. Clapham, K. Abdullah, J.J. Jeswiet, P.M. Wild, and R. Rogge, Neutron Diffraction Residual Stress Mapping in Same Gauge and Differential Gauge Tailor-Welded Blanks, *J. Mater. Proc. Tech.*, 2004, **148**, p 177–185